Proposal and Verification of a Kinetic Mechanism Model for NO_x Removal with Hydrazine Hydrate

Liu Hong, Li-Jie Yin, and De-Zhen Chen
Thermal & Environmental Engineering Institute, Tongji University, Shanghai 200092, China

Du Wang
Thermal & Environmental Engineering Institute, Tongji University, Shanghai 200092, China

Institute of Energy and Environment Engineering, Shanghai University of Electric Power, Shanghai 200090, China

DOI 10.1002/aic.14688
Published online November 28, 2014 in Wiley Online Library (wileyonlinelibrary.com)

A relatively precise kinetic mechanism of NO_x reduction using $N_2H_4{\cdot}H_2O$ in a selective non-catalytic reduction process was proposed and verified by experiment in this study. The dominant radicals and reactions were confirmed, and the proper ranges of key parameters were determined through sensitivity analysis. Both experimental and simulation results show that the effective temperatures exhibit a bimodal distribution with the optimum temperatures being approximately 893 and 1248 K and the lower temperature window falling in the range of 848–973 K. The optimum residence time of the reaction was 0.2–0.35 s under the research conditions, and a longer residence time would lead to the regeneration of NO_x. The normalized stoichiometric ratio (NSR) of 3.0 corresponded to the lowest temperature window, and a higher NSR value would make the temperature window shift to a higher temperature range. This kinetic mechanism model for the $N_2H_4{\cdot}H_2O$-based De-NO_x process will serve its precise application. © 2014 American Institute of Chemical Engineers *AIChE J*, 61: 904–912, 2015

Keywords: hydrazine hydrate ($N_2H_4{\cdot}H_2O$), NO_x, selective non-catalytic reduction, kinetic mechanism model, sensitivity analysis

Introduction

Selective noncatalytic reduction (SNCR) De-NO_x technology has been used to reduce nitrogen oxide (NO_x) emissions from flue gas for nearly 30 years.[1] In the SNCR process, a gaseous or dissolved reagent (ammonia, urea, isocyanic acid, etc.) is injected into the hot exhaust gases of stationary combustion systems in the presence of a certain level of oxygen to initiate a sequence of reactions that converts NO_x to molecular nitrogen (N_2).[2] However, the traditional SNCR De-NO_x reagents only work in a narrow temperature window roughly between 1100 and 1400 K, during which the O_2 level is around 4–8 V/V% for coal-fired boilers. This narrow temperature window reduces the effective reaction range, and the averaged De-NO_x efficiency is only approximately 30% according to the practical operation log, which cannot meet the rigid emission limitations.[3–5] In addition, the traditional reagents such as ammonia and urea are not suitable for SNCR NO_x removal from flue gas of lower temperatures and higher O_2 contents, which is occurring widely in practice, for example, the temperature of flue gas exhausted from iron ore sintering bed may not higher than 500°C while its O_2 level could be higher than 10 V/V%,[6] yet its NO_x emission is strictly controlled[7]; another example is the flue gas from incinerators, it often contains more extra O_2 but is of lower temperature than that from coal-fired boilers yet its NO_x emission limits become similarly stricter.[8] To meet the emission limitations,[9] selective catalytic reduction De-NO_x technology is widely used in a much lower temperature range (250–400°C),[10–12] but NO_x reduction based on an SNCR process at lower temperatures is more desirable due to its much lower cost and more convenient operation.[13]

Hydrazine hydrate ($N_2H_4{\cdot}H_2O$) is a type of strong reducing agent that is widely used as a rocket propellant, pesticide material, an oxygen scavenger in boiler water, and so forth. The compound $N_2H_4{\cdot}H_2O$ has been tentatively used as a De-NO_x reagent at moderate temperatures in bench-scale experiments conducted by Azuhata et al.[13] The results showed that NO was reduced to N_2 and H_2O by N_2H_4 in the temperature range of 773–873 K and that the presence of O_2 prohibited the reduction of NO_x. Lee and Kim[14] tested the NO_x reduction with hydrazine in a pilot-scale reactor and found that hydrazine had an effective De-NO_x effect in the temperature range of 800–950 K, which was approximately 300 K lower than that of ammonia. Diesen et al.[15] found that the NH_2 radical plays the most important role in the SNCR process, and the generation of the NH_2 radical is the key elementary reaction, which is similar to the thermal De-NO_x mechanism with ammonia and the NO_x OUT mechanism with urea. The differences are that the NH_2 radical is

Additional Supporting Information may be found in the online version of this article.

Correspondence concerning this article should be addressed to D.Z. Chen at chendezhen@tongji.edu.cn

generated by a cleavage reaction of the N—N bond in the N_2H_4 molecule, instead of the N—H bond in ammonia and of the C—N bond in urea.[1,16] The average bond energy of the N—N bond (251.04 kJ/mol) is lower than that of the N—H bond (368.19 kJ/mol) and the C—N bond (338.90 kJ/mol),[17] which means that the activation energy for the N_2H_4 decomposition reaction is lower than that of ammonia and urea molecules, indicating that this reaction can occur at a lower temperature. Consequently, the De-NO_x mechanism of hydrazine hydrate can be divided into two steps: the production of NH_2 radicals by thermal decomposition and oxidation of N_2H_4 molecules, and the De-NO_x mechanism between the NH_2 radical and NO_x.

Although $N_2H_4{\cdot}H_2O$ can work well at moderate temperatures, to date it has not been widely used in industrial processes. One of the main reasons is that the mechanism of the reaction kinetics for the reductive reactions has not been sufficiently clarified. To study the chemical kinetic mechanism of the $N_2H_4{\cdot}H_2O$-based De-NO_x process, many researchers have conducted experimental studies,[13,14] but the detailed mechanism of SNCR De-NO_x reactions has not yet been obtained.

To understand the behaviors of $N_2H_4{\cdot}H_2O$ decomposition, some simple models for describing its thermal decomposition process were proposed based on experimental data obtained from certain temperature ranges,[15,18,19] but none of those models can describe the whole reaction process and match the experimental data well. In 2011, Konnov and De Ruyck[20] proposed a detailed decomposition mechanism of hydrazine in inert gases that includes 11 species and 51 elementary reactions; the authors surmised that the initial decomposition reaction of hydrazine into two NH_2 radicals and the subsequent reactions between hydrazine and NH_2 radical govern the hydrazine decomposition reactions and that the NH_2 radical plays the most important role in the decomposition process of hydrazine. Considering the influence of oxygen, Shen[21] proposed a model with 21 species and 125 elementary reactions for the N/H/O reaction system to describe the decomposition process of hydrazine.

To investigate the De-NO_x mechanism between the NH_2 radical and NO_x, a so-called Miller and Bowman (M&B) model with 53 reactant species and 251 reactions was proposed by Miller and Bowman[1] to describe the SNCR process based on ammonia, this system includes the reactions between NH_3 and NO in the SNCR process and the NO formation reactions in the combustion process. Several reaction rate coefficients of this model were later modified by Miller and Glarborg.[22]

Taking into account both the thermal decomposition of $N_2H_4{\cdot}H_2O$ and the reaction between NH_2 radical and NO_x, some rough models for predicting NO_x reduction with hydrazine were proposed, but the SNCR De-NO_x efficiencies predicted by these models were much greater than the experimental data.[23,24] Later a more detailed model for hydrazine-based SNCR process with 24 species and 113 elementary reactions was proposed by Hong et al.,[25] by which NO reduction trends as a function of temperature was predicted and matched the pilot-scale experimental data well, but there was a distinct gap between the computational results and the experimental data because the operational conditions of the experimental reactor were far from a perfectly stirred reactor (PSR), which neglects the influence of the mixing process of the flue gas and reductants. Moreover, some of the elementary reactions adopted in this model directly taken from the thermal De-NO_x mechanism of ammonia in the temperature range from 1100 to 1400 K, which is quite different from the De-NO_x temperature window of hydrazine hydrate (750–1050 K). Therefore, to develop a more precise model, some reaction rate coefficients of the elementary reactions in the model had to be modified.

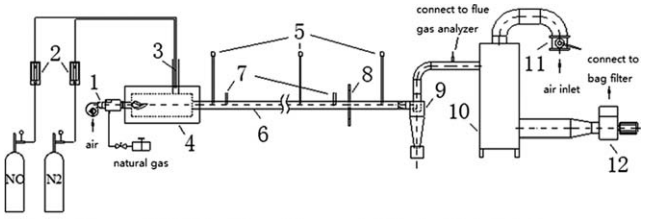

1 Burner; 2 Flowmeter; 3 NO, N_2 inlet; 4 Furnace; 5 Thermocouple; 6 Flue pipe; 7 Hydrazine feeder;
8 High temperature flow meter; 9 Cyclone; 10 Cold air mixing tank; 11 Damper; 12 Draft fan

Figure 1. Schematic diagram of the SNCR experimental setup.

(1 Burner; 2 Flow meter; 3 NO, N_2 inlet; 4 Furnace; 5 Thermocouple; 6 Flue gas pipe; 7 Hydrazine feeder; 8 High temperature flow meter; 9 Cyclone; 10 Cold air mixing tank; 11 Damper; 12 Draft fan).

Here, a more precise model describing the N_2H_4—NO_x—O_2 reactions was proposed, and the model was used to simulate the actual $N_2H_4{\cdot}H_2O$-based De-NO_x process in a bench scale experiment setup with help of Chemkin/Fluent. The simulation results were compared with the experimental data. Additionally, critical influencing factors (residence time, normalized stoichiometric ratio [NSR], etc.) were investigated through a sensitivity analysis. The flue gas produced in the experimental setup was characterized with high O_2 contents varying in the range of 9.8–15.8 V/V%. The influence of O_2 content in the flue gas on $N_2H_4{\cdot}H_2O$-based De-NO_x efficiency has been studied in previous work, which showed that the decrease in O_2 content would move the effective De-NO_x temperature window to the higher temperature region, but the De-NO efficiency is almost unaffected.[25] In this research, the O_2 contents in the flue gas were remained in its natural values to investigate the De-NO_x behaviors under higher O_2 contents.

Materials and Methods

Experimental setup

The experimental reactor system for $N_2H_4{\cdot}H_2O$-based NO_x reduction is shown in Figure 1. The reactor wall is insulated to maintain a nearly stable temperature distribution in the reactor. The total flow rate of the flue gas varied from 62.8 to 98.2 Nm^3/h. A solution of $N_2H_4{\cdot}H_2O$ was sprayed into the stream of combustion products through two atomizing nozzles installed in a pilot-scale pipe flow reactor. To measure the dosage of the De-NO_x reagent, the NSR was defined as

$$\mathrm{NSR}=\frac{\text{actual amount of De-NO}_x\text{ reagent}}{\text{stoichiometrically required reagent for De-NO}_x} \quad (1)$$

The flue gas contained approximately 150 ppmv CO, 10 V/V% H_2O and 3 V/V% CO_2. The N_2 was added into the chamber of the furnace to regulate the O_2 level in the flue gas. A group of thermocouples were installed at intervals of 1 m along the reactor pipe to measure the temperature distribution of the flue gas in the reactor. The O_2 content in the flue gas increased from 9.8 to 15.8 V/V% as the temperature

Table 1. Modified Kinetic Parameters of Elementary Reactions

Reaction	A (cm^3/mol s)	n	E (kJ/mol)
R32. $NH_2+OH=NH+H_2O$	5.0E11	0.50	8.32
R33. $NH_2+NO=NNH+OH$	8.9E12	−0.35	0
R58. $NH_2+O_2=HNO+OH$	2.0E12	0.00	62.36
R114. $NO+OH+M=HONO+M$	5.1E23	−2.51	−0.28

decreased from 1271 to 780 K. Within this temperature range, more than 90% of the NO_x exists in form of NO; therefore, NO was used to replace NO_x in later discussions. The inlet concentration of NO varied from 320 to 580 ppmv and increased with the increase in temperature. Considering the incomplete contact between the flue gas and the De-NO_x reagent, the NSR value used in the experiment varied from 1.5 to 4.0. The variation of NSR value is realized by changing the concentration of $N_2H_4{\cdot}H_2O$ in the solution while the flow rate of the reagent solution is controlled to be constant to avoid the disturbance of the temperature field in the reactor caused by difference in NSR values. A GASMET DX4000 type FT/IR gas analyzer (Temet, Finland) and a KM9106 type gas analyzer (Kane, UK) were used to measure the concentrations of NO, NO_2, O_2, and so forth along the reactor. A PGM-7800 multiple gas analyzer (RAE Systems, USA) was used to monitor the concentration of NH_3 to detect the "ammonia slip," and a PGM-7240 VOC analyzer (RAE Systems, USA) was used to monitor the N_2H_4 slip.

Mathematical model

Sensitivity analysis is used to consider the impact of variables on the dependent variables.[26] It is defined as

$$S_i=\frac{k_i}{F(k_i)}\frac{\partial F(k_i)}{\partial k_i}=\frac{\partial \ln\left(F(k_i)\right)}{\partial \ln\left(k_i\right)} \tag{2}$$

where S_i is the local sensitivity coefficient of the ith reaction to the target function, F is the target function (NO concentration in this research study), and k_i is the rate coefficient of the ith reaction. The absolute value of S_i represents the degree of impact. The larger the absolute value is, the greater the effect on the target function is. If S_i is negative, the reaction will promote NO reduction; on the contrary, if S_i is positive, the reaction will enhance NO formation.

In this study, sensitivity analysis was used to study the influences of the reactions on the De-NO_x efficiency to determine elementary reactions composing the model, and 25 species and 114 reactions (which are listed in Supporting Information, Appendix) were embodied in the final model to describe the SNCR process based on hydrazine hydrate. According to the local sensitivity analysis, the reactions of R32, R33, and R58 are the most sensitive reactions to NO concentration in the classical SNCR mechanism, but the reaction rate coefficients of R32, R33, and R58 applied in the classical SNCR process could not match the $N_2H_4{\cdot}H_2O$-based SNCR process as they have different temperature windows.[1,22] So, the reaction rate coefficients of R32, R33, and R58 were modified based on a kinetic model of the NH_2 + NO reactions as shown in Table 1. Meanwhile, OH radical plays a key role in the $N_2H_4{\cdot}H_2O$-based reaction process, the reaction between OH and NO, which was not included in the classical kinetic reaction mechanism, should be considered here. Therefore, a new reaction, R114 was introduced based on the previous model.[27,28]

During the simulation process, the gas flow field, heat transfer, and reactions were considered simultaneously, and the general form of the governing equation is defined as

$$\mathrm{div}(\rho u\phi)=\mathrm{div}(\Gamma \mathrm{grad}\phi)+S \tag{3}$$

where φ represents different variables in different equations, ρ is the density in kg/m^3, u is the velocity in m/s, and S is the source term. The specific forms of φ, Γ, and S in the different governing equations are listed in Table 2. The standard $k-\varepsilon$ model was applied to describe the influence of turbulence on the flow field of the gas in the reactor, and the P-1 model was adopted to describe the radiation heat transfer of the flue gas.[29,30]

The constants in the governing equations are as follows

$$C_{1\varepsilon}=1.44, C_{2\varepsilon}=1.92, C_\mu=0.09, \sigma_k=1.0, \sigma_\varepsilon=1.3 \tag{4}$$

The parameter S_e in the energy conservation equation is the source term resulting from the following reaction

$$S_e=\sum_i w_i\Delta h_i \tag{5}$$

where w_i is the ith reaction rate and Δh_i is the enthalpy change of the ith reaction.

The NH_2—NO reactions, thermal decomposition and oxidation mechanism of hydrazine hydrate are integrated in this study, as shown in the Supporting Information, Appendix. The reaction rate of the ith elementary reaction can be calculated by

$$w_i=k_i\prod_{j=1}^{n}C_j^{\alpha_j} \tag{6}$$

$$k_i=A_rT^{\beta_r}\exp\left(-E_r/RT\right) \tag{7}$$

Table 2. Equations Governing the Standard $k-\varepsilon$ Model

Equation	φ	Γ	S
Continuity	1	0	0
X-momentum	U	$\mu_{\mathrm{eff}}=\mu+\mu_t$	$-\frac{\partial p}{\partial x}+\frac{\partial}{\partial x}\left(\mu_{\mathrm{eff}}\frac{\partial u}{\partial x}\right)+\frac{\partial}{\partial y}\left(\mu_{\mathrm{eff}}\frac{\partial v}{\partial x}\right)+\frac{\partial}{\partial z}\left(\mu_{\mathrm{eff}}\frac{\partial w}{\partial x}\right)$
Y-momentum	V	$\mu_{\mathrm{eff}}=\mu+\mu_t$	$-\frac{\partial p}{\partial y}+\frac{\partial}{\partial x}\left(\mu_{\mathrm{eff}}\frac{\partial u}{\partial y}\right)+\frac{\partial}{\partial y}\left(\mu_{\mathrm{eff}}\frac{\partial v}{\partial y}\right)+\frac{\partial}{\partial z}\left(\mu_{\mathrm{eff}}\frac{\partial w}{\partial y}\right)$
Z-momentum	W	$\mu_{\mathrm{eff}}=\mu+\mu_t$	$-\frac{\partial p}{\partial z}+\frac{\partial}{\partial x}\left(\mu_{\mathrm{eff}}\frac{\partial u}{\partial z}\right)+\frac{\partial}{\partial y}\left(\mu_{\mathrm{eff}}\frac{\partial v}{\partial z}\right)+\frac{\partial}{\partial z}\left(\mu_{\mathrm{eff}}\frac{\partial w}{\partial z}\right)$
Turbulent kinetic energy	K	$\mu+\frac{\mu_t}{\sigma_k}$	$G_k+\rho\varepsilon$
Rate of viscous dissipation	ε	$\mu+\frac{\mu_t}{\sigma_\varepsilon}$	$\frac{\varepsilon}{k}(C_{1\varepsilon}G_k-C_{2\varepsilon}\rho\varepsilon)$
Energy	T	$\frac{\mu}{\mathrm{Pr}}+\frac{\mu_t}{\sigma_T}$	S_e
Species	Y_n	$D_n+\frac{\nu_t}{\mathrm{Sc}_t}$	S_n

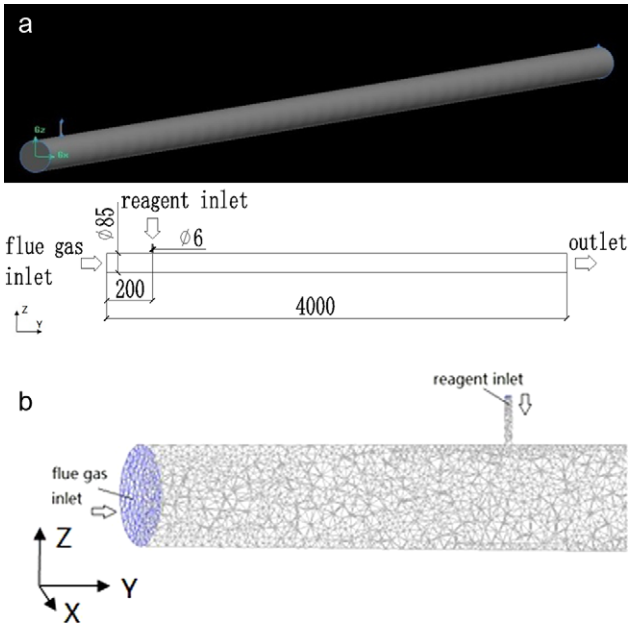

Figure 2. Structure scheme and reactor grid.

(a) Three-dimensional model and vertical section sketch of the flue-pipe reactor (unit: mm), (b) tetrahedral meshes of the inlet section of the flue-pipe reactor. [Color figure can be viewed in the online issue, which is available at wileyonlinelibrary.com.]

where C_j is the molar concentration of the reactants in mol/m^3, n is the number of the reactants species, k_i is the reaction rate coefficient of the ith reaction, α_j is the exponent of reactant. In the Chemkin software, the default value of α is the stoichiometric number of the reactant in simple reactions,[31–33] A_r is the pre-exponential factor in cm^3/mol s, β_r is the temperature exponent, E_r is the activation energy of the reaction in kJ/mol, and R is the gas constant. The detailed values of the aforementioned parameters are listed in the Supporting Information, Appendix.

Chemkin/Fluent coupled model

The PSR model in Chemkin was used to simulate the reaction under ideal mixing conditions. Considering the influence of the diffusion process of the reductant in the flue gas, Computational fluid dynamics (CFD) simulations were used to simulate the flow field inside the reactor. The Chemkin/Fluent model was used to simulate the actual De-NO_x process based on the experimental reactor. The structure scheme and grid of the reactor are shown in Figure 2. The initial and boundary conditions were set according to the experimental conditions.

The simulation study was conducted by importing the reaction mechanism file and the operating conditions of the experiments, including the composition and flux of the flue gas, the initial concentration of the reductants, the reaction temperature, and so forth into the chemical kinetics software Chemkin and the CFD software Fluent to start the simulation.

Results and Discussion

Experimental results and discussion

The De-NO efficiency η was calculated by

$$\eta = 1 - \frac{[NO]_{out}}{[NO]_{in}} \tag{8}$$

where $[NO]_{in}$ and $[NO]_{out}$ are the volume fractions of NO at the inlet and outlet, respectively. In the experiments it was found more than 95% of the NO_x existed in the form of NO; therefore Eq. (8) also gave the De-NO_x efficiencies.

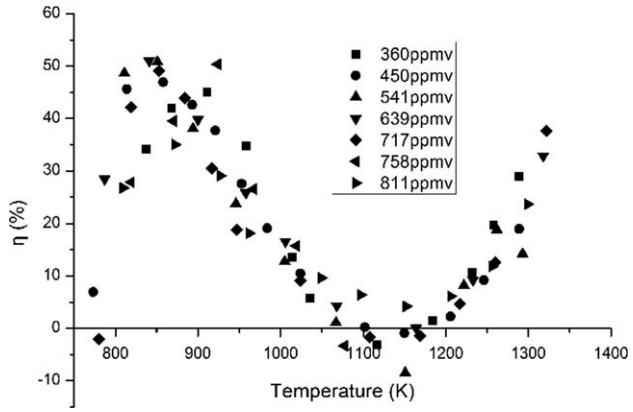

Figure 3. De-NO efficiency of SNCR experiments as a function of temperature.

Initial condition: O_2 content, 9.8% (higher temperature) to 15.8% (lower temperature); NSR = 4.0.

Figure 3 shows the De-NO efficiency as a function of temperature for different concentrations of the inlet NO. The results show that the De-NO efficiency shows a bimodal behavior with temperature: the lower temperature window is from 820 to 960 K, and this window corresponds to higher efficiencies than those found for the higher temperature zone. When the initial NO concentration increased from 360 to 811 ppmv, the temperature windows shows little change, which indicates that the NO concentration has little effect on the De-NO efficiency. Additionally, it is worth mentioning that no "ammonia slip" (ammonia emission from the reactor) or "N_2H_4 slip" (N_2H_4 emission from the reactor) was detected throughout hydrazine-based SNCR experiments.

Simulation results and discussion

Comparison of the De-NO_x Efficiency Between the Simulations and Experiments. Figure 4 shows the variations of the De-NO_x efficiency η as a function of the reaction temperature and depicts the comparison of the experimental data with the simulation results based on the Chemkin/Fluent coupled model. The De-NO_x efficiency was calculated using Eq. 8.

The solid line in Figure 4 shows the simulation result for a PSR model in Chemkin. The two dashed lines refer to the

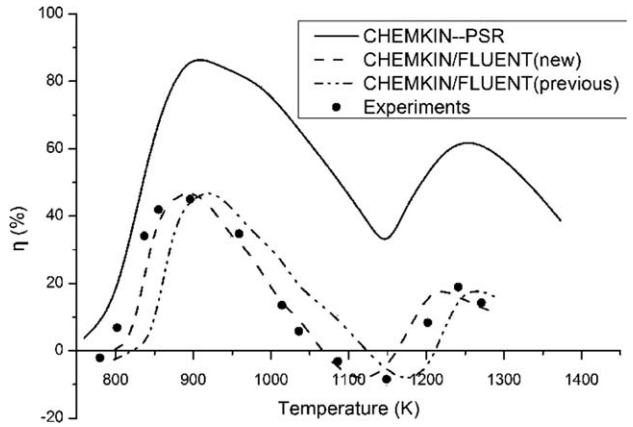

Figure 4. Comparison of De-NO_x efficiency between simulations and experiments.

Initial conditions: NO_{in} = 450 ppmv (900 K), NSR = 4.0, O_2 content: 9.8% (1271 K) to 15.8% (780 K).

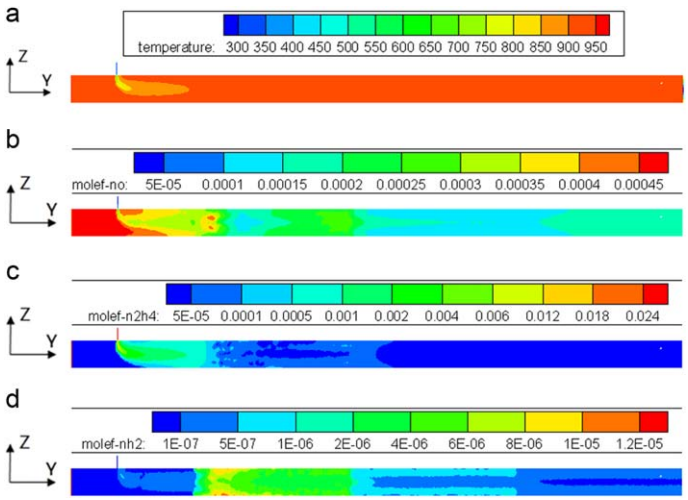

Figure 5. Distributions of temperature and molar fractions of gas species (adiabatic wall).

Initial conditions: Tf = 923 K, Tr = 300 K, NSR = 4.0, adiabatic wall. (a) Distribution of temperature in the reactor, (b) concentration of NO, (c) concentration of N_2H_4, (d) concentration of NH_2 radical. [Color figure can be viewed in the online issue, which is available at wileyonlinelibrary.com.]

simulation results of the Chemkin/Fluent coupling simulations obtained by embedding the previous and improved De-NO_x mechanism into Fluent. As illustrated by the data shown in Figure 4, the results of the kinetics calculations using only the PSR model in Chemkin showed bimodal temperature behaviors for SNCR De-NO_x with hydrazine hydrate, and the trend in the De-NO efficiency as a function of the temperature distributions is in well agreement with the trend obtained from the experiment data. However, there is a large gap between the simulation results and the experimental data due to the mixing and heat transfer process in the reactor was ignored in the PSR model. In contrast, the results from the Chemkin/Fluent coupling simulations adopting both the previous model (marked previous) and the new model in this research (marked new) are very close to the experimental data. The new model proposed here is more precise and matched perfectly with the experimental data, especially at the lower temperature window of 837–961 K,

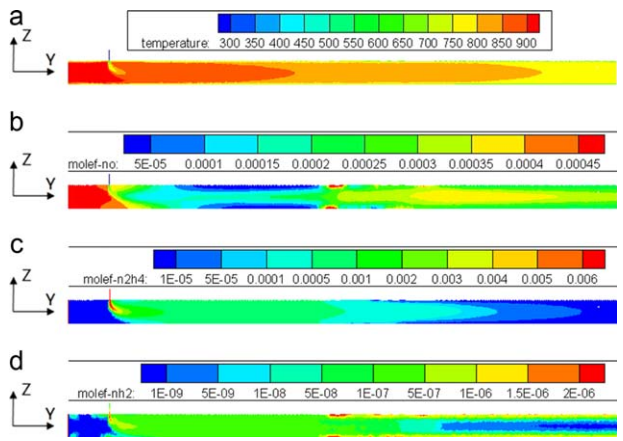

Figure 6. Distributions of temperature and molar fractions of gas species (nonadiabatic wall).

Initial conditions: Tf = 923 K, Tr = 300 K, NSR = 4.0, nonadiabatic wall (qw = 950 W/m^2). (a) Distribution of temperature in the reactor, (b) concentration of NO, (c) concentration of N_2H_4, (d) Concentration of NH_2 radical. [Color figure can be viewed in the online issue, which is available at wileyonlinelibrary.com.]

where the peak value of the De-NO efficiency reached 47.8%. However, the simulation results based on the previous mechanism shifted the temperature window to a higher temperature by approximately 30 K. Compared with the PSR model adopted in Chemkin, the CFD simulation with the De-NO_x mechanism embedded could predict the actual SNCR De-NO_x process more precisely. Meanwhile, as shown in Figures 5 and 6, the Chemkin/Fluent coupled models could also describe the mixing and heat transfer processes between the flue gas and the reductants in the reactor precisely; therefore, the improved De-NO_x mechanism proposed in the new model in this research is applicable to the $N_2H_4{\cdot}H_2O$-based De-NO_x process.

Both experiment and simulation results showed bimodal temperature behaviors of $N_2H_4{\cdot}H_2O$-based SNCR De-NO_x process, this is because different elementary reactions dominate the SNCR process in different temperature ranges. In the lower temperature window (820–960 K), the dominant reactions of De-NO_x mainly includes branching reactions of NH_2+NO such as R33 and R34, the competition reactions of NNH such as R37 and R39, and decomposition of N_2H_4, that is, R87 and so forth (see the Supporting Information, Appendix). According to the expression of reaction rate coefficient in Eq. 7, as the temperature increases, the reaction rate of R87 increases, but those of R33 and R34 decrease, and those of R37 and R39 remain constants. Consequently, the optimal temperature for De-NO_x appears in the lower temperature window 820–960 K. In the higher temperature window (1250–1330 K), the reactions R88, R90, and R93 producing NH_3 are activated; and the De-NO_x reaction mechanism is fairly similar to that of the classical NH_3-based SNCR process, except that the De-NO_x efficiency is lower at the same NSR value, due to the fact that only part of $N_2H_4{\cdot}H_2O$ could transform into NH_3 successfully through reactions R88, R90, and R93; while the rest of $N_2H_4{\cdot}H_2O$ is oxidized to produce N_2, NO, and so forth at higher temperatures.[20,21]

Distributions of Temperature and NO Inside the Reactor. Figure 5 shows the distributions of the temperature and concentration of several dominant reactants in the reactor. The initial temperatures of the flue gas and reagents are 923 and

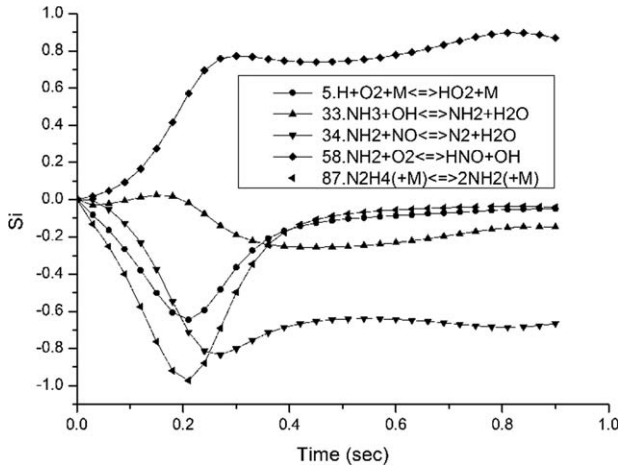

Figure 7. Influence of the residence time on the sensitivity coefficients of NO.

Initial conditions: Tf = 923 K, NSR = 4.0, PSR model (Chemkin).

300 K, respectively, the velocity of the flue gas and reagent are 9.48 and 11.47 m/s, respectively, the NSR value is 4.0, and the wall of the reactor was set to be adiabatic.

As shown in Figure 5a, the spraying of a reagent only slightly affects the temperature distribution near the reagent inlet region; the temperature distribution of the reactor appears relatively stable. Figures 5b, c, d show the concentrations of NO, N_2H_4, and NH_2 radicals in the reactor, respectively. These figures show that the reagent N_2H_4 decomposes rapidly after being sprayed into the reactor; a large number of NH_2 radicals are generated in the middle region of the reactor and then take part in the De-NO_x reaction. The NO concentration decreases rapidly from 450 ppmv at the inlet to approximately 100 ppmv at the outlet. Near the outlet, the NO concentration increases slightly because the NH_2 radicals have disappeared, as shown in Figure 5d; and other nitrogenous radicals such as N_2O and HNO would generate NO through reactions R25 and R43 under oxidizing conditions.

Combining the length of the reactor with the velocity of the flue gas, the time to complete the De-NO_x reaction was estimated to be approximately 0.4 s at 923 K. If the residence time is too long, additional NO will generate through reactions R25 and R43 under the temperature of 923 K. Due to heat loss, the temperature of the tubular reactor actually decreases with the flow of flue gas, when the boundary conditions adopted for the simulations are in total agreement with the actual conditions in the experiments, the following parameters should be adopted for the reactor wall based on the heat loss measured in the experiments

$$\delta=0.053,\lambda=0.127,q_w=950 \tag{9}$$

where δ is the thickness of the reactor wall in m; λ is the thermal conductivity of the reactor wall in W/m K; and q_w is the thermal flux through the reactor wall in W/m^2. The new distributions of temperature and NO, N_2H_4, NH_2 concentrations in the reactor are illustrated in Figure 6.

As shown in Figure 6a, the temperature of the flue gas in the reactor decreases gradually with the flow of flue gas from 923 K at the inlet to 800 K at the outlet when the wall was set to be nonadiabatic, which is identical to the measured results. Figure 6b shows that the distribution of the NO concentration in the reactor is a little different from that in Figure 5b, and that the NO concentration is less than 150 ppmv in the middle of reactor but increased to 230 ppmv at the outlet, showing a distinct NO reformation near the outlet of the reactor. This is due to the further decease of NH_2 radicals at the outlet, as shown in Figures 6c and d, N_2H_4 decomposes rapidly after being sprayed into the reactor; at the same time a large number of NH_2 radicals are generated in the middle region of the reactor and exhausted at the outlet, and the concentrations of N_2H_4 and NH_2 were 1.91 and 0.45 ppmv at the outlet of reactor, respectively; which are even lower than those outlet concentrations in Figures 5c and d (4.35 and 1.18 ppmv, respectively). Compared to temperature distribution shown in Figure 6a, temperature distribution shown in Figure 5a is closer to the optimal De-NO_x temperature, which is around 900 K as shown in Figure 4; therefore, to maintain the temperature of the reactor around the optimal De-NO_x temperature is important to obtain a lower NO_x emission.

Influence of Residence Time on De-NO_x Efficiency. Since NO formation reactions and De-NO_x reactions occur simultaneously in the reactor, but the reaction rates of these two types of reactions may change with the residence time and temperature. To optimize the De-NO_x process, the appropriate residence time should be determined under certain conditions (e.g., under a known temperature distribution). For this purpose, the local sensitivity analysis was applied based on PSR model in the Chemkin software, the PSR model of reactor is set to be adiabatic to avoid the influence caused by the variation of temperature. According to sensitivity to the NO concentration, five elementary reactions were selected for local sensitivity analysis. The results were given in Figure 7 at the temperature of 923 K.

As shown in Figure 7, the sensitivity coefficients of R5, R34, and R87 decrease with an increase in the residence time and reach their minimum values at approximately 0.2–0.25 s. This means that the most vigorous De-NO_x reactions occur within this time period. At residence times rose from 0.25 to 0.35 s, the coefficients of R5, R34, and R87 to the NO concentration remain negative but approach to zero; while that of R33 decreased and R58 increased. Due to the comprehensive influence of all of the reactions, the De-NO_x efficiency of the system becomes relatively stable. When the residence time is longer than 0.35 s, the sensitivity

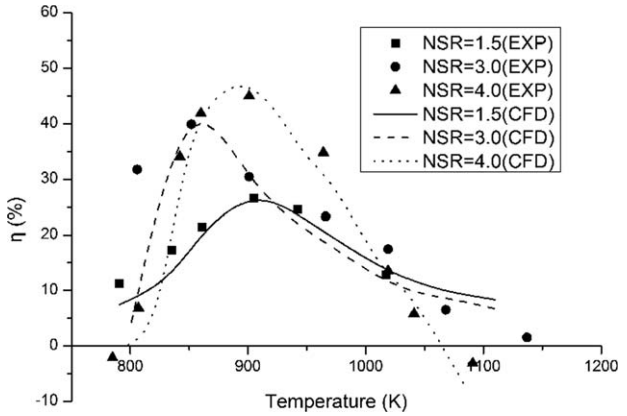

Figure 8. Influence of NSR on De-NO_x efficiency.

Initial conditions: NSR = 1.54.0, O_2 content: 13.5% (higher temperature) = 16.9% (lower temperature).

Table 3. Sensitivity Coefficients of NO at Different NSR Values

	Temperature (K)	833			857			893			956			1018		
	NSR	1.5	3.0	4.0	1.5	3.0	4.0	1.5	3.0	4.0	1.5	3.0	4.0	1.5	3.0	4.0
S_i	5.H+O_2+M<=>HO_2+M	−1.283	−1.935	−2.267	−1.892	−3.265	−3.464	−3.424	−3.083	−3.283	−1.517	−1.436	−1.290	−0.678	−0.636	−0.710
	33.NH_3+OH<=>NH_2+H_2O	−0.043	−0.320	−0.399	0.009	0.046	0.202	−0.017	−0.885	−1.510	−1.467	−1.837	−1.983	−1.687	−2.208	−2.311
	34.NH_2+NO<=>N_2+H_2O	0.105	0.157	0.020	−0.207	−0.902	−0.936	−1.942	−5.192	−5.830	−4.412	−5.134	−5.392	−4.236	−5.462	−5.710
	58.NH_2+O_2<=>HNO+OH	0.060	0.291	0.240	0.220	0.775	1.636	1.596	5.203	6.277	5.007	5.839	6.305	4.976	6.888	7.358
	87.N_2H_4(+M)<=>$2NH_2$(+M)	−0.555	−1.767	−1.697	−1.142	−2.984	−2.713	−2.871	−3.763	−3.960	−0.226	−0.378	−0.287	0.026	0.319	−0.549
	114. NO+OH+M = HONO+M	−0.021	−0.058	−0.065	−0.055	−0.089	−0.121	−0.087	−0.154	−0.258	−0.358	−0.684	−0.855	−0.756	−0.942	−1.259

coefficients of reactions R58 remain very positive with the absolute values higher than those of R34, which is the most important De-NO_x reaction; while the sensitivity coefficients of R87, the NH_2 formation reaction, increased slightly to approach zero; therefore, the average concentration of NO increased at the outlet of the reactor as a consequence of N_2H_4 disappearing and preponderance of NH_2 oxidation at approximately 0.4 s of residence time. So the optimum residence time is the time of reaching the minimum NO concentration; and for the reaction conditions in this research, the optimum residence time was found to be about 0.2–0.35 s by the simulation results.

Influence of NSR Value on De-NO_x Efficiency. In the SNCR De-NO_x process, the NSR value greatly affects the efficiency of NO reduction. To study the effect of the NSR value on De-NO_x efficiency, the SNCR processes with different NSR values were simulated, and the results are shown in Figure 8.

It can be seen that when the NSR value increases from 1.5 to 3.0, the peak value of De-NO_x efficiency increases from 19.8 to 40.5%, the temperature window expands remarkably on both sides, and the optimal temperature decreases from 906 to 850 K. When the NSR increases from 3.0 to 4.0, the peak value of De-NO_x efficiency increases from 40.5 to 45.8%, the temperature window shifts to the higher temperature side, and the optimal temperature increases from 850 to 898 K. Therefore, the NSR value of 3.0 corresponds to the lowest temperature window. When the NSR value is 1.5, the De-NO_x efficiency predicted by the simulation is slightly lower than experimental data. The reason is that, when the gas phase heat-transfer model was applied for the flow field simulation, the latent heat of vaporization of the reagent solutions was neglected by some assumptions in the simulations, which leads to the initial temperature of the flue gas in the experiments being higher than that of the CFD simulations.

The influence of the NSR value on the De-NO_x efficiency at five dominant temperatures in the lower temperature window of hydrazine hydrate by local sensitivity analysis is shown in Table 3.

As shown in Table 3, as the NSR value increases from 1.5 to 3.0, the sensitivity coefficients of the five dominant reactions for NO generation, with the exception of R58, greatly decreases. The De-NO_x efficiency of the reactor thus increases significantly, and the temperature window remarkably expands on both sides. As the NSR value increases from 3.0 to 4.0, divergence appears in the variations of the sensitivity coefficients for the reactions at different temperature conditions. At lower temperature conditions, such as 833 and 857 K, the sensitivity coefficients of the six reactions to the NO concentration remain generally stable; however, at the higher temperature region from 893 to 1018 K, the sensitivity coefficients of the five dominant reactions, excluding R58, clearly decreased. Therefore, as temperature increases from 893 to 1018 K, increasing the NSR value from 3.0 to 4.0 can promote the De-NO_x process significantly, as illustrated in Figure 8.

Influence of CO/H_2O/CO_2 on De-NO_x Efficiency. The influences of CO, H_2O, and CO_2 on the De-NO_x efficiency of SNCR process are accounted in the reactions such as R2, R11, R109, R110, R111, R112, and R113, as shown in the Supporting Information, Appendix, and the effects of these seven reactions on the De-NO_x efficiency are shown by local

Table 4. Sensitivity Coefficients of $CO/H_2O/CO_2$ Associated Reactions on NO Content at Different Temperatures

Temperature (K)		833	857	893	956	1018
S_i	2. $OH+H_2=H_2O+H$	0.007	0	0.020	−0.005	0.013
	11. $H+OH+M=H_2O+M$	0.015	0	−0.001	0	0
	109. $CO+O+M=CO_2+M$	0.046	0	0	0	0
	110. $CO+OH=CO_2+H$	−0.216	−0.046	0.028	−0.032	0.007
	111. $CO+O_2=CO_2+O$	0	0	0	0	0
	112. $CO+HO_2=CO_2+OH$	0.083	0	0	0	0
	113. $NO_2+CO=CO_2+NO$	0	0	0	0	0

sensitivity analysis at five different temperatures within the lower temperature window, as listed in Table 4.

As can be seen in Table 4, the sensitivity coefficients of these seven reactions are very close to zero and much smaller than those of the dominant reactions listed in Table 3. That is to say, these reactions had negligible impacts on the De-NO_x process under the research conditions, and the corresponding species, namely CO, H_2O, and CO_2 also play fairly minor roles in the SNCR process based on $N_2H_4{\cdot}H_2O$.

Conclusions

The comparison of the simulated and experimental results for the hydrazine hydrate-based SNCR process was performed in this study, and the following conclusions can be drawn:

A more precise kinetics mechanism model for the N_2H_4—NO_x—O_2 reactions was proposed and verified by comparing the simulation results with pilot-scale experimental results. This model is found applicable to simulate the $N_2H_4{\cdot}H_2O$-based De-NO_x process and can predict the De-NO_x efficiency accurately.

The experimental results show that the effective temperatures of the $N_2H_4.H_2O$-based SNCR process are bimodally distributed: the lower temperature window was from 820 to 960 K, and the higher temperature window was from 1260 to 1330 K. The temperature windows change little with different inlet NO concentrations.

The simulation results show that the lower temperature window should be from 848 to 973 K, the optimum temperature of NO_x reduction is 898 K, and the maximum De-NO_x efficiency is 47.8% under the experimental conditions with NSR being around 4.0, which is in satisfactory agreement with the experiment results.

The appropriate residence time for De-NO_x reactions was within the range of 0.2–0.35 s. The regeneration of NO_x will occur if the residence time is more than 0.4 s under this research conditions.

The NSR value plays an important role in the $N_2H_4{\cdot}H_2O$-based SNCR De-NO_x process. The temperature window was remarkably expanded as the NSR value increases from 1.5 to 3.0; as the NSR value varies from 3.0 to 4.0, a higher De-NO_x efficiency was attained, but the temperature window also shifted to higher temperatures.

Under present conditions, the influence of CO, H_2O and CO_2 on the SNCR process is very negligible.

Acknowledgment

This research was supported by the National Natural Science Foundation of China (NSFC)-Bao Steel Joint research fund (Grant No. 50874134).

Notation

A_r = pre-exponential factor, cm^3/mol s.
C = constant.
C_r = molar concentration of reactants, mol/m^3.
E_r = activation energy of reaction, kJ/mol.
F = target function.
k = turbulent kinetic energy, m^2/s^2.
k_i = rate coefficient of the ith reaction.
q_w = heat flux through the reactor wall, W/m^2.
R = gas constant.
S = source term.
Sc_t = Schmidt number.
S_e = source term in energy conservation equation.
S_i = partial sensitivity coefficient of the ith reaction.
T_f = temperature of flue gas.
T_r = temperature of reagents.
w_i = reaction rate of the ith reaction, mol/cm^3 s.

Greek letters

α = reaction exponent.
β_r = temperature exponent.
δ = thickness of wall, m.
ε = turbulent dissipation rate, m^2/s^3.
η = De-NO efficiency.
λ = thermal conductivity of wall, W/m·K.
μ_t = turbulent kinetic viscosity, Pa/s.
ν_t = turbulent kinematic viscosity, m^2/s.
μ_{eff} = effective kinetic viscosity, Pa/s.
σ_T = Prandtl number.
φ = global variable
Γ = diffusion coefficient.
Δh_n = enthalpy change of the nth reaction, J/mol.

Subscripts and superscripts

e = energy conservation equation.
eff = effective.
f = flue gas.
i = the ith reaction.
j = stoichiometric number of reactant.
in = inlet.
out = outlet.
p = pressure.
r = reaction, reagents.
t = turbulent.

Literature Cited

1. Miller JA, Bowman CT. Mechanism and modeling of nitrogen chemistry in combustion. *Prog Energy Combust*. 1989;15:287–338.
2. Duo WK, Dam-Johansen K, Østergaard K. *Widening the temperature range of the thermal DeNO$_x$ process*. An experimental investigation. 23rd Symposium (Int.) on Combustion, Pittsburgh, 1990.
3. Fan WY, Zhu TL, Sun YF, Lv D. Effects of gas compositions on NO_x reduction by selective non-catalytic reduction with ammonia in a simulated cement precalciner atmosphere. *Chemosphere*. 2014;113:182–187.
4. Yang J, Ma HT, Yamamoto Y, Yu J, Xu GW, Zhang ZG, Suzuki Y. SCR catalyst coated on low-cost monolith support for flue gas denitration of industrial furnaces. *Chem Eng J*. 2013;230:513–521.

5. Salimian S, Hanson RK. A kinetic study of NO removal from combustion gases by injection of NH_i-containing compounds. *Combust Sci Technol*. 1980;23:225–230.
6. Fan XH, Yu ZY, Gan M, Li, WQ, Ji ZY. Influence of O_2 content in circulating flue gas on iron ore sintering. *Int J Iron Steel Res*. 2013; 20(6):1–6.
7. MEP and AQSIQ, 2012. *Emission Standard of Air Pollutants for Sintering and Pelletizing of Iron and Steel Industry*. (GB 28662-2012). Beijing (in Chinese): Gov. Print. Office.
8. MEP and AQSIQ, 2014. *Standard for Pollution Control on the Municipal Solid Waste Incineration*. (GB 18485-2014). Beijing (in Chinese): Gov. Print. Office.
9. MEP and AQSIQ, 2011. *Emission Standard of Air Pollutants for Thermal Power Plants*. (GB 13223-2011). Beijing (in Chinese): Gov. Print. Office.
10. Fissore D, Tejedor DG, Barresi AA. Experimental investigation of the SCR of NO_x in a simulated moving bed reactor. *AIChE J*. 2006; 52(9):3146–3154.
11. Kota AS, Luss D, Balakotaiah V. Modeling studies of low-temperature aerobic NO_x reduction by a sequence of LNT-SCR catalysts. *AIChE J*. 2013;59(9):3421–3431.
12. Tamm S, Olsson L, Fogel S, Gabrielsson P, Skoglundh M. A kinetic model of the hydrogen assisted selective catalytic reduction of NO with ammonia over Ag/Al_2O_3. *AIChE J*. 2013;59(11):4325–4333.
13. Azuhata S, Akimoto H, Hishinuma Y. Effect of H_2O_2 on homogeneous gas phase NO reduction reaction with NH_3. *AIChE J*. 1982; 28(7):7–11.
14. Lee JB, Kim SD. NO_x reduction by hydrazine in a pilot-scale reactor. *Chem Eng J*. 1998;69(2):99–104.
15. Diesen RW. Mass spectral studies of kinetics behind shock waves. II. Thermal decomposition of hydrazine. *J Chem Phys*. 1963;39(9): 2121–2128.
16. Rota R, Antos D, Zanoelo EF, Morbidelli M. Experimental and modeling analysis of NO_x OUT process. *Chem Eng Sci*. 2002;57(1):27–38.
17. Sanderson RT. *Chemical Bonds and Bond Energy*, 2nd ed. New York: Academic Press, 1976.
18. Gilbert M. Kinetics of hydrazine decomposition in a laminar non-isothermal flow. *Combust Flame*. 1958;2(2):149–156.
19. Ghosh PK, Bair EJ. Reactions of nitrogen-hydrogen radicals. II. Decomposition of hydrazine by hydrogen atoms. *J Chem Phys*. 1966;45(12):4738–4741.
20. Konnov AA, De Ruyck J. Kinetic modeling of the decomposition and flames of hydrazine. *Combust Flame*. 2001;124(1–2):106–126.
21. Shen CH. *The Analysis of Thermal Dissociation of Hydrazine*, Ph. D. Dissertation, Tainan City, Taiwan: National Cheng Kung University, 2004, pp. 79–95.
22. Miller JA, Glarborg P. Modeling the thermal De-NO_x process: closing in on a final solution. *Int J Chem Kinetics*. 1999;31(11):757–765.
23. Zhang ZM, Chen DZ. *Kinetics Analysis of Reactions Between Hydrazine and NO in Flue Gas Under Moderate to High Temperature*. Chinese Society of Engineering Thermophysics, Combustion Science Conference, Wuhan, China, 2006, pp. 890–896 (in Chinese).
24. Cho YH, Chang HM. A kinetic model for the reduction of nitric oxide by hydrazine. *KSME Int J*. 1997;11(4):428–434.
25. Hong L, Chen DZ, Wang D, Huang S. Kinetic mechanism and characteristics researches for hydrazine-based NO_x removal at moderate to high temperatures. *Environ Sci*. 2012;33(8):2901–2908 (in Chinese).
26. Saltelli A, Chan K, Scott EM. *Sensitivity analysis*, Vol. 134. New York: Wiley, 2000.
27. Glarborg P, Miller JA, Kee RJ. Kinetic modeling and sensitivity analysis of nitrogen oxide formation in well-stirred reactors. *Combust Flame*. 1986;65:177–202.
28. Diau EW, Yu T, Wagner MAG, Lin MC. Kinetics of the $NH_2 + NO$ reaction: effects of temperature on the total rate constant and the OH/H_2O branching ratio. *J Phys Chem*. 1994;98(15):4034–404.
29. Sazhin SS, Sazhina EM, Faltsi-Saravelou O, Wild P. The P-1 model for thermal radiation transfer: advantages and limitations. *Fuel*. 1996;75(3):289–294.
30. Habibi A, Merci B, Heynderickx GJ. Impact of radiation models in CFD simulations of steam cracking furnaces. *Comput Chem Eng*. 2007;31(11):1389–1406.
31. Kee RJ, Miller JA, Jefferson TH. *CHEMKIN: A General-Purpose, Problem-Independent, Transportable, Fortran Chemical Kinetics Code Package*. Sandia Laborotaries Report, 1980, SAND80–8003.
32. Kee RJ, Rupley FM, Miller JA. *CHEMKIN—II: a Fortran Chemical Kinetics Package for the Analysis of Gas-Phase Chemical Kinetic*. Sandia Laborotaries Report, 1989, SAND89–8009.
33. Kee RJ, Rupley FM, Meeks K, Miller JA. *CHEMKIN—III: A Fortran Chemical Kinetics Package for the Analysis of Gas-Phase Chemical and Plasma Kinetic*, Sandia Laborotaries Report, 1996, SAND96–8216.
34. Miller JA, Kee RJ. Chemical nonequilibrium effects in hydrogen-air laminar jet diffusion flames. *J Phys Chem*. 1977;81(25):2534–2542.
35. Miller JA, Branch C, Kee RJ. A chemical kinetic model for the selective reduction of nitric oxide by ammonia. *Combust Flame*. 1981;43:81–98.
36. Catoire L, Luche J, Dupré G, Paillard C. Critical reactions for the hydrazine vapor detonations. *Shock Waves*. 2001;11(2):97–103.

Manuscript received June 2, 2014, and revision received Oct. 14, 2014.